A&A 470, 1193–1199 (2007)
DOI: 10.1051/0004-6361:20077472

Astronomy & Astrophysics

On the dynamical stability of the Rosetta orbiter. II.

E. Mysen and K. Aksnes

Institute of Theoretical Astrophysics, University of Oslo, PO Box 1029 Blindern, 0315 Oslo, Norway
e-mail: [eirik.mysen;kaare.aksnes]@astro.uio.no

Received 14 March 2007 / Accepted 31 May 2007

ABSTRACT

In an orbit around a comet, a spacecraft is subject to several spin-orbit resonances. These enhanced couplings, induced by the rotation of the nucleus, by temporal variations in the outgassing pressure field and, at last, by a rotation of the probe's solar cell arrays, are systematically mapped in this paper. Using the simplified pendulum model, each resonance overlap problem is one-parametric. For the gravitational resonances, the boundary between shape stable and shape unstable cometocentric orbits is well formulated by a simple law in a parameter range which includes an adopted nominal Rosetta scenario. Stability conditions are discussed for each problem.

Key words. celestial mechanics – space vehicles – comets: individual: 67P/Churyumov-Gerasimenko – methods: analytical – methods: numerical

1. Introduction

The Rosetta probe will study comet 67P/Churyumov-Gerasimenko from a bound orbit in 2014–2015. For the delivery of the lander Philae to the comet's surface, trajectories with perihelia close to the comet's anticipated highly non-spherical nucleus have been suggested for Rosetta. Also, the extrapolation of the details in the comet nucleus' gravity field by monitoring the spacecraft's radio carrier waves, as part of the Rosetta Radio Science Investigations (Pätzold et al. 2006), requires a close orbit for extended periods of time. At such near approaches, the part of the comet's gravity field which is modulated by the nucleus rotation induce spin-orbit resonances, their interaction again leading to large aperiodic and, to a certain extent, unpredictable changes in the shape of the spacecraft's orbit (Olsen 2005; Mysen et al. 2006). We therefore here present a simple, but systematic analysis of the location of the resonance overlap regions and their sensitivity to intrinsic and controllable parameters. The nucleus rotation is assumed to be uniaxial.

As the comet rotates, the physical characteristics of its inner coma change in a way which is not trivially connected to the surface properties of the nucleus (Crifo & Rodionov 1997). Nevertheless, for orbits in the plane normal to the cometocentric direction of the Sun, a simple law for the time-varying outgassing pressure field around the comet might be of acceptable precision. As a result, the resonance problem can be treated within the Hamiltonian formalism and the implications are explored.

Spin-orbit resonances are also induced when Rosetta's exceptionally large solar cell arrays are rotated with respect to the Sun. Such a spacecraft spin reduces the power collected by the arrays, but decreases the secular dynamical effects of radiation pressure so that passive orbit stability is improved, as long as the resonance overlap regions are avoided. These regions are mapped below using the same formalism as for the gravity field and outgassing pressure.

2. A simplified resonance theory

We will begin by briefly reviewing the simplest resonance model, the pendulum. Let the Hamiltonian of our system be represented by

$$F = F_0 + V_1, \quad F_0 = -\frac{\mu_c}{2a} \tag{1}$$

with F_0 as the energy of Keplerian motion, μ_c as the product of the constant of gravitation and nucleus mass and a as the semi-major axis of the probe's cometocentric orbit. The perturbing potential V_1 yields the perturbing acceleration $\delta\ddot{\boldsymbol{r}}$ through the use of the gradient, $\delta\ddot{\boldsymbol{r}} = -\nabla V_1$.

First, assume that this potential is periodic in the spacecraft's mean orbit anomaly $\tilde{l}$ and one rotation angle θ, describing either the rotation phase of the comet nucleus or the spacecraft, dependent on the problem at hand. The perturbing potential can then be Fourier expanded according to

$$V_1 = A_S + \sum_{j,k} A_{jk} \cos \hat{l}_{jk} \tag{2}$$

where

$$\hat{l}_{jk} = j\theta - k\tilde{l} + \varphi_{jk}(g,h), \quad k = 1,2,3,... \tag{3}$$

and j is an integer which will be specified later for each problem. The phase φ_{jk} is a function of the slowly changing variables g, the orbit's argument of pericenter, and h, the orbit's longitude of ascending node.

According to perturbation theory, the mean state of the system is well represented by $F = F_0 + A_S$ for limited periods of time since the fast angles θ and $\tilde{l}$, at least in comparison to g and h, make all A_{jk} terms oscillate rapidly and therefore quickly average out to zero. However, for certain orbits, the time derivative of $\hat{l}_{jk}$ could be small so that the associated component should not be removed a priori on the basis of such a qualitative argument. Let the center of this resonance be defined by

$$\dot{\hat{l}}_{jk} \approx j\omega - k\dot{\tilde{l}} \equiv 0, \quad \omega = \dot{\theta} \tag{4}$$

which by Kepler's third law, $\dot{\hat{l}}^2 = \mu_c\, a^{-3}$, gives us the semi-major axis a_R of the resonance center

$$a_R = \kappa\, k^{2/3}, \quad \kappa \equiv \left(\frac{\mu_c}{j^2\omega^2}\right)^{1/3}. \tag{5}$$

In Mysen et al. (2006) it is shown that if $A_R \equiv A_{jk}$ and $\hat{l} = \hat{l}_{jk}$ are the resonant amplitude and angle, respectively, then the function

$$\Delta F = \frac{1}{2}W(\Delta a)^2 - A_R \cos\hat{l}, \quad W \equiv \frac{3}{4}\frac{\mu_c}{a_R^3} \tag{6}$$

is conserved for a near a_R such that $\Delta a \equiv a - a_R$ is small, see also Olsen (2005).

If the amplitude A_R of the pendulum Hamiltonian Eq. (6) is assumed to be constant, it can be reasoned that the maximum semi-major axis distance which the system can wander away from a_R to either side without escaping the resonance is given by

$$\Delta a_k = 2\left(\frac{|A_R|}{W}\right)^{1/2} = \frac{4}{\sqrt{3}}\left(\frac{a_R^3}{\mu_c}|A_R|\right)^{1/2}. \tag{7}$$

More details and information on the resonances' topology and first order corrections of their positions are given in Mysen et al. (2006). These include aspects which are not incorporated in the presented analysis, something which makes the problem easier to address in a general way. This choice can partly be justified by the expected low precision of the resonance overlap criterion for orbit shape instability.

3. Gravitational resonances

The gravitational potential can be expanded in spherical harmonic functions according to (Heiskanen & Moritz 1967)

$$\begin{aligned} V_1 \;=\; & \frac{\mu_c}{r}\sum_{n=2}^{\infty}\sum_{m=0}^{n}\left(\frac{r_c}{r}\right)^n P_{nm}(\sin\beta) \\ & \times[\, c_{nm}\cos m\lambda + s_{nm}\sin m\lambda\,] \end{aligned} \tag{8}$$

with r_c as a reference radius usually set equal to the typical radius of the central object, and r as the distance from the nucleus mass center to the point where the potential is to be evaluated. The north latitude and east longitude of this point are given by β and λ, respectively, while c_{nm} and s_{nm} are field expansion coefficients. The Legendre functions are given by P_{nm}.

Defining our reference XY-plane to coincide with the plane normal to the nucleus spin and rotation axis, we have the more convenient form

$$\begin{aligned} V_1 \;=\; & \frac{\mu_c}{r}\sum_{n,m}\sum_{q}\left(\frac{r_c}{r}\right)^n \sqrt{c_{nm}^2 + s_{nm}^2}\,\Theta_n^{(mq)}(I) \\ & \times\cos\left[m(\theta - h) - q(f + g) + \varphi_{nmq}\right] \end{aligned} \tag{9}$$

from Mysen et al. (2006) which is based on Kinoshita et al. (1974). Here, the inclination I of the spacecraft's orbit is relative to the plane normal to the rotation axis, θ is the rotation phase of the comet nucleus and f is the probe's true orbit anomaly. The orbit's longitude of ascending node h and argument of pericenter g are calculated relative to the plane from which the inclination is measured, and relative to some cometocentric non-rotating X-axis lying in the same plane. At last, the integer q takes on the values $q = \pm n, \pm(n-2), \pm(n-4), ...$

3.1. Second harmonics

In the principal axis (Goldstein 1980) mass centered system of the comet nucleus, only c_{20} and c_{22} of the second harmonics are different from zero. If then the true anomaly is replaced by a series expansion in mean anomaly, see for instance Olsen (2005) and Mysen et al. (2006), convergent for $e \lesssim 0.65$, one has for the strength of the pendulum Eq. (6) with resonant angle Eq. (3)

$$A_R = \frac{\mu_c}{a}\left(\frac{r_c}{a}\right)^2 c_{22}\,\Theta_2^{(22)}(I)\,Q_k(e), \quad j = 2 \tag{10}$$

where j and k are the integers of Eq. (5), the inclination function is

$$\Theta_2^{(22)} = \frac{3}{4}(1 + \cos I)^2, \tag{11}$$

and

$$Q_k = \frac{1}{\pi}\int_0^{2\pi} \mathrm{d}\tilde{l}\left(\frac{a}{r}\right)^3 \cos 2f\cos k\tilde{l}. \tag{12}$$

Throughout this paper, the values of integrals like Eq. (12) are evaluated numerically on a dense grid of eccentricities, and form the coefficients of Fourier series meant to approximate certain functions of true anomaly which the potential consists of, see Eq. (9). The correspondence between these functions and their Fourier series has been extensively tested and verified.

At large eccentricities $e \gtrsim 0.5$ there are some non-negligible corrections of the amplitude Eq. (10) linked to expansion series like Eq. (12), but with $\cos 2f \to 1$. Some of these have a different dependency on the inclination, $\sim\sin^2 I$ (Mysen et al. 2006), and are not included in what follows. The amplitude Eq. (10) also suffers from the assumption that $\cos 2f$ in Eq. (12) should be replaceable by $\sin 2f$ and still give the same result, an approximation which is not always appropriate at large e's.

Under these assumptions the resonance width to one side of the center $a_R(k)$ goes as, see Eq. (7)

$$\Delta a_k = \alpha\sqrt{|Q_k|}, \quad \alpha = r_c 2\sqrt{|c_{22}|}\,(1 + \cos I). \tag{13}$$

Neighbouring resonances with centers $a_R(k)$ and $a_R(k+1)$ overlap at an eccentricity e_k

$$\Delta a_k(e_k) + \Delta a_{k+1}(e_k) = a_R(k+1) - a_R(k) \tag{14}$$

or

$$\sqrt{|Q_k(e_k)|} + \sqrt{|Q_{k+1}(e_k)|} = \frac{\kappa}{\alpha}[(k+1)^{2/3} - k^{2/3}], \tag{15}$$

yielding $e_k = e_k(\kappa/\alpha)$. If the trajectories are less elliptic than e_k, they should be "safe" with some reservations related to the roughness of the resonance overlap criterion for chaos.

Based on our knowledge of the solutions of Eq. (15) the function

$$\Omega_k = a_k\frac{1 - e_k}{1 + e_k} = \frac{q_k}{1 + e_k}, \tag{16}$$

with a_k as the semi-major axis where the resonances overlap, is defined, or in more explicit form

$$\frac{\Omega_k}{\alpha} \equiv \frac{1 - e_k}{1 + e_k}\left[\frac{\kappa}{\alpha}k^{2/3} + \sqrt{|Q_k(e_k)|}\right], \tag{17}$$

where the latter ratio also is a function of κ/α only since e_k is. The ratio is plotted for $k = 5$, 10, 15 and 20 in Fig. 1 where the

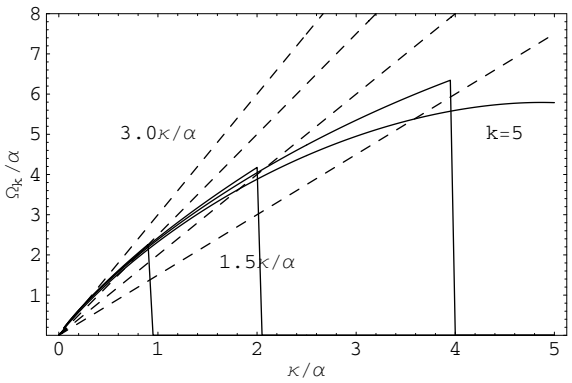

Fig. 1. The closest approach distance parameter Ω_k for regular orbits scaled to the resonance strength parameter α, as a function of nucleus mass/rotation parameter κ relative to α. From top to bottom represented by the solid curves: $k = 20$, 15, 10 and at last 5 as indicated. The linear dashed curves with slopes 1.5, 2.0, 2.5 and 3.0 are included for reference.

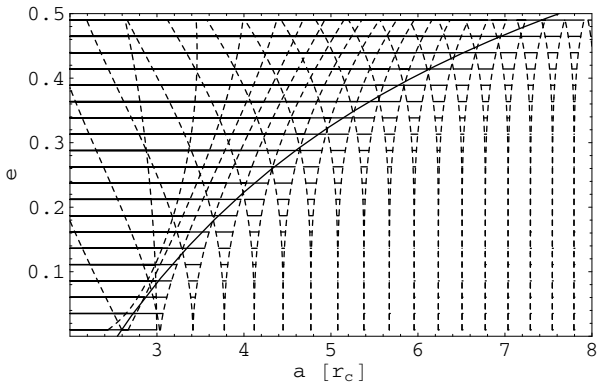

Fig. 2. The widths of the resonances for what is here (only) adopted as a nominal Rosetta scenario are shown for a prograde orbit lying in the spin plane. The solid line is given by $\Omega_{10}(1 + e) = a(1 - e)$.

Table 1. Intrinsic and controllable parameters which in this paper are taken as nominal: constant of gravitation times nucleus mass factor μ_c, mean radius r_c, rotation period, the resonance location parameter κ, defined value of gravity coefficient and maximum resonance strength parameter α.

μ_c	r_c	$2\pi\omega^{-1}$	$\kappa_{j=2}$	$\lvert c_{22}\rvert$	$\alpha(I = 0)$
$1.1\, r_c^3\, h^{-2}$	1.98 km	12.3 h	1.0	0.1	$1.3\, r_c$

solid curves are defined to drop to zero when $e_k > 0.5$, for which this paper's simplifications are of limited value.

There are two interesting points to note from the plot. First of all, for $\kappa/\alpha \lesssim 2{-}3$, this ratio is fairly independent of k, and a single curve $\Omega_k = \Omega$ in Eq. (16) defines well all resonance crossings. Secondly, note that each function Ω_k is well presented by a quadratic least-squares fit on the form

$$\frac{\Omega_k}{\alpha} \sim \Omega_{1,k} \left(\frac{\kappa}{\alpha}\right) + \Omega_{2,k} \left(\frac{\kappa}{\alpha}\right)^2 . \tag{18}$$

As long as we restrict our attention to orbit eccentricities $e < 0.5$ and resonance strengths $\alpha \gtrsim \kappa/5$, the orbits which are described by Ω_{10} could be adopted as transition trajectories, a stability criterion which becomes more conservative with decreasing α. This, one can claim since whenever large k resonances cross in our studied region, $e < 0.5$, they are well represented by Ω_{10}. Accordingly, "safe" trajectories should fulfill

$$\frac{q}{1+e} \equiv \Omega > \Omega_{10} \approx 2.53\,\kappa - 0.24\,\kappa^2/\alpha, \tag{19}$$

again with emphasis on the restrictions

$$e < 0.5, \quad \alpha \gtrsim \kappa/5 \tag{20}$$

where the eccentricity limit is set not only for needs of resonance amplitude modifications, but also because the necessary Fourier series expansions in mean anomaly eventually diverge. From Eq. (19), one can then conclude that systems with low κ are desirable in the sense that they allow closer approaches without inducing changes in the orbit's shape. On the other hand, for low κ, the orbit stability is more difficult to improve by choosing more inclined orbits, Eq. (13), since Ω is more insensitive to α. Table 1 gives some parameters, based on Lamy et al. (2003) and Davidsson & Gutiérrez (2005), Kossacki & Szutowicz (2006) and Rickman et al. (1987) which we in in this paper only adopt as nominal. These values place a nominal Rosetta scenario in a parameter region where the aforementioned conclusions are applicable. For instance, little improvement in the closest "safe" approach distance can be expected by an inclination increase from $I \sim 0$ to $\pi/2$ since κ^2/α only increases from 0.8 to 1.6.

Figure 2 shows the resonance widths in semi-major axis and eccentricity space for the parameters of Table 1 and inclination $I_R = 0$, and demonstrates $\Omega_k \approx \Omega \equiv \Omega_{10} = 2.54\, r_c$, represented by the solid line. This value is somewhat different from that given by Eq. (19), which is due to the role of the latter as representative for a wide parameter range.

At last in this section we show the results of simulations for directly prograde orbits around a nominal nucleus, corresponding to the scenario of Fig. 2. As throughout this paper, we use a numerical differential equation solver package with an LSODA approach, switching between a non-stiff Adams method and a stiff Gear backward differentiation formula method, as is default in Wolfram's "Mathematica 5.2" software. We have compared simulations using this package with results from double precision Fortran 90 Bulirsch-Stoer (Stoer & Bulirsch 1980) simulations of the gravity problem in this section, and found that the package yields predictions which are precise enough for the applications in this paper. The plot Fig. 3 shows the difference in semi-major axis before and after the probe passes its pericenter for a series of simulations at different initial eccentricities, to the extent that such a change can be defined. The stability boundaries in semi-major axis for the different eccentricities as given by Eq. (19) are represented by vertical bars in the plot, and yield acceptable results. Continuation of the series to the left results in semi-major axis variations which are completely off the given scale and are therefore not included, while roughly to the right of the bars, Δa is only a measure of the difference in phase of a periodic variation. Note also that the law seems to have some applicability for higher eccentricities than what we have a theoretical foundation to claim. For plots of the semi-major axis as a function of time, the reader is referred to Mysen et al. (2006).

3.2. Irregular nucleus shape

For bodies which are triaxial ellipsoids with constant mass density, i.e. are regular, all odd n components of Eq. (8) vanish. However, there seems to be evidence for some degree of irregularity (Muinonen & Lagerros 1998), and the effect of the $n = 3$ order of the field is therefore explored here.

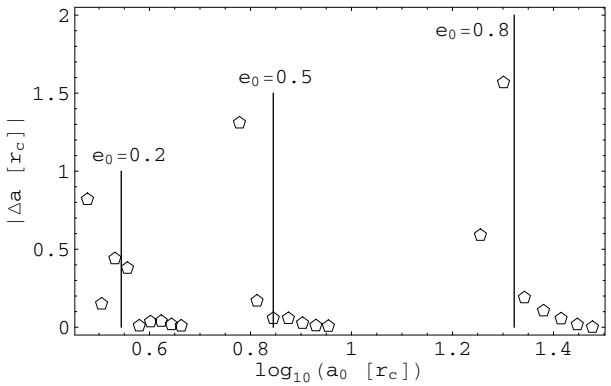

Fig. 3. The changes in the probe orbit's semi-major axis over a pericenter passage, represented by the polygons, are shown as functions of the initial semi-major axes. The initial argument of pericenter g_0, longitude of ascending node h_0 and inclination I_0 of the orbit with respect to the plane normal to the rotation axis are set to the same value, $I_0 = g_0 = h_0 = 0$. We have set the only non-zero higher order gravity coefficients of the simulations to $c_{20} = -c_{22} = 0.1$, defining the scale r_c.

Again, removing the true anomaly from the expansion Eq. (9) in the same way as in the previous section, one gets for the absolute value of the resonance angle Eq. (3)'s amplitude

$$|A_R| = \frac{\mu_c}{a}\left(\frac{r_c}{a}\right)^3 \sqrt{c_{3m}^2 + s_{3m}^2}\,\Theta_3^{(mq)}(I)|R_k^{(q)}(e)| \tag{21}$$

where $j = m = 1, 2, 3$ of Eq. (5) are relevant. The eccentricity dependent function $R_k^{(q)}$ is given by

$$R_k^{(q)} = \frac{1}{\pi}\int_0^{2\pi} \mathrm{d}\tilde{l}\left(\frac{a}{r}\right)^4 \cos qf \cos k\tilde{l}, \tag{22}$$

yielding the $|A_R|$ above under similar assumptions as described in the previous section on the second harmonics, i.e. modifications should be expected at large eccentricities. While Eq. (21) gives resonance half widths which, unlike those of the second harmonics, decrease with semi-major axis $\Delta a \sim a_R^{-1/2}$, this reduction is not so substantial that they can be ignored if the central body is very irregular, i.e. if c_{3m} or s_{3m} is large.

More quantitatively, the resonance half width goes as

$$\Delta a_k = \frac{\gamma}{\sqrt{a_R(k)}}\sqrt{|R_k^{(q)}|} \tag{23}$$

where

$$\gamma \equiv \frac{4}{\sqrt{3}} r_c^{3/2}\,(c_{3m}^2 + s_{3m}^2)^{1/4}\,\sqrt{|\Theta_3^{(mq)}|}. \tag{24}$$

Now, the resonances which are of particular interest are those which are strong at a large distance away from the nucleus. That is, resonances with small m and large q's of Eq. (21), see Eq. (22), could lead to modifications of the orbit shape stability a great distance away from the central body. Assuming that these resonances exist at a location where those generated by the second harmonics are of less importance, it is meaningful to address the isolated overlap problem for a given m and q of the third harmonics, see Eq. (14)

$$k^{-1/3}\sqrt{|R_k^{(q)}(e_k)|} + (k+1)^{-1/3}\sqrt{|R_{k+1}^{(q)}(e_k)|} = \frac{\kappa^{3/2}}{\gamma}\left[(k+1)^{2/3} - k^{2/3}\right]. \tag{25}$$

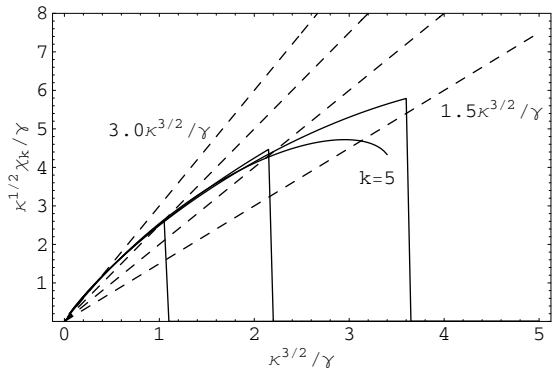

Fig. 4. The scaled approach distance χ_k is shown as a function of a ratio consisting of the resonance strength parameter γ and resonance location parameter κ. The index k takes on the values 5, 10, 15 and 20.

In a similar way as in Eq. (16) with $\Omega_k \to \chi_k$, it is interesting to investigate the quantity

$$\frac{\kappa^{1/2}}{\gamma}\chi_k = \frac{\kappa^{1/2}}{\gamma}\frac{1-e_k}{1+e_k}\left[\kappa k^{2/3} + \frac{\gamma}{\sqrt{a_R(k)}}\sqrt{|R_k^{(q)}(e_k)|}\right] = \frac{1-e_k}{1+e_k}\left[\frac{\kappa^{3/2}}{\gamma}k^{2/3} + \frac{\sqrt{|R_k^{(q)}(e_k)|}}{k^{1/3}}\right] \tag{26}$$

which is a function of $\kappa^{3/2}/\gamma$ since e_k is. Figure 4 shows the ratio Eq. (26) with the hazardous combination $j = 1$ and $q = 3$, plotted as a function of this variable for $k = 5$, 10, 15 and 20. Again, the curves are set to zero when $e_k > 0.5$ and our approximations are questionable. The $k = 5$ curve, which is the one which dips the most in the plot, does not experience $e_k > 0.5$ in our chosen parameter range, but is nevertheless truncated since $|R_5^{(3)}|$ begins to decrease with increasing eccentricity beyond the point of truncation. That is, the inner resonances separate. From the figure one can clearly see that this problem is even better described by a law $\chi_k = \chi$ for $\kappa^{3/2}/\gamma \lesssim 2{-}3$. If specific values are required, one can use $\chi \approx \chi_{10}$ with

$$\chi_{10} \approx 2.76\,\kappa - 0.33\,\kappa^{5/2}/\gamma, \quad \gamma \gtrsim \kappa^{3/2}/4 \tag{27}$$

remembering that $\chi = a\,(1-e)/(1+e) > \chi_{10}$ represents the safe side of the boundary. It is very important to note that in this case $\kappa = \kappa(j = m = 1)$ is possible, unlike for the second harmonics which have $\kappa = \kappa(j = 2)$ only. This means that the resonances could cross a larger distance away from the nucleus than do the second harmonics, i.e. $\kappa(j = 1) = 1.6\,r_c$ from Table 1, but also that the former are closer to the "safer" non-linear region if γ and α are comparable. The parameter γ can be reduced by avoiding orbits in the polar region since (Kinoshita et al. 1974):

$$\Theta_3^{(m3)} = \frac{15}{16}(1+\cos I)\sin^2 I, \quad m = j = 1 \tag{28}$$

$$\Theta_3^{(m3)} = \frac{15}{8}(1+\cos I)^2 \sin I, \quad m = j = 2. \tag{29}$$

Again we conclude the section with some results from series of simulations which are compared to Eq. (27), in very much the same way as in Fig. 3. Here, however, we have chosen a polar orbit $I_0 = \pi/2$ with only the coefficients $c_{31} = -s_{31} \equiv 0.1$ of the higher order gravity field as different from zero, an unphysical definition which is adopted in order to test Eq. (27) more precisely. This gives us a resonance strength $\gamma = 0.84\,r_c^{3/2}$

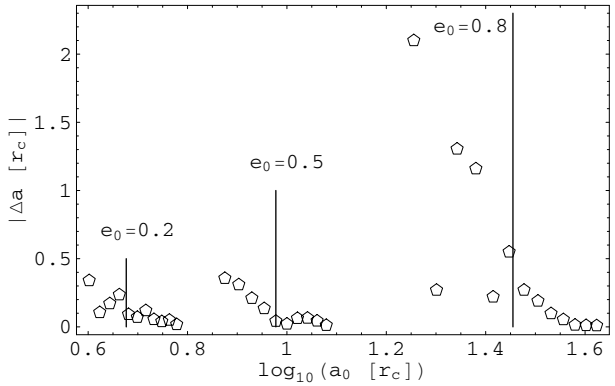

Fig. 5. The plot shows results from three different simulation series which are separated by the initial eccentricity. For each initial eccentricity value the initial semi-major axis is varied, and the difference in semi-major axis before and after pericenter passage is mapped. These results are then compared to what is predicted by Eq. (27), represented by the vertical bars. The orbit is polar $I_0 = \pi/2$ in order to make $\Theta_3^{(13)}$ large, and $g_0 = h_0 = 0$.

of Eq. (24), and a χ_{10} of Eq. (27) of $\chi_{10} = 3.16\, r_c$ which is compared to the simulation results in Fig. 5. Although this time our predictions are more off than in Fig. 3, something is clearly happening in their vicinity. A generalization of the law to $e = 0.8$ does not seem to compromise its applicability.

4. Outgassing

It is expected that the Rosetta target 67P/Churyumov-Gerasimenko is active during all phases of the mission (Fulle et al. 2004), but that this activity is significantly increased after the onset of water sublimation between $R = 3$–4 AU. From existing studies it seems difficult to be conclusive when it comes to formulating a force law for the resulting outgassing pressure on an orbiting spacecraft, which is informative, see Mysen & Aksnes (2006). However, the hypothesis that the pressure field drops in strength as the inverse square of the distance from some geometrical center of the nucleus was put forth in the referenced (our) work, and that the force under a range of controllable conditions acted mostly away from the nucleus.

What seems to be an unresolved issue of great interest and relevance to the Rosetta mission is the level of precision of a possible inverse square statistical law. Below, we shall allow the field to be modulated by the rotation of the nucleus, where it is assumed that the variations are dominated by the base frequency which is given by the rotation period of the comet. However, one should note that if the form of the comet nucleus is that of a triaxial ellipsoid, it is possible that the temporal variations of the pressure field are dominated by a frequency twice that given by the rotation period of the nucleus since the comet-Sun geometry then repeats itself twice for every rotation cycle of the comet nucleus.

The variations in the pressure field caused by the rotation of the nucleus can then be interpreted as statistical fluctuations around a law. In the following, another and more restrictive assumption will be that for an orbit with a given radius, the strength of the field will not change, except as stated above. According to some simple models of the coma gas dynamics, it is possible that this assumption is of acceptable precision (see for instance Mysen & Aksnes 2006, and references therein) in the so-called solar plane-of-sky, i.e. the plane normal to the cometocentric direction of the Sun. That is, the pressure field is not, or only weakly, a function of the spacecraft's position except through the inverse square dependency on distance. Some simulations of comae (Crifo et al. 2004) indicate that, before the onset of water sublimation, the pressure field could be of a more isotropic nature, and that the analysis below therefore is more applicable for general orbits in such cases.

All in all, we have for the perturbing acceleration

$$\delta\ddot{\boldsymbol{r}} = \Gamma(t)\frac{\boldsymbol{r}}{r^3}, \quad V_1 = \Gamma\frac{1}{r}, \quad \Gamma \neq \Gamma(\boldsymbol{r}) \tag{30}$$

where the explicit time dependency of the pressure field is through $\theta \sim t$, a rotation phase of the nucleus

$$\Gamma = \Gamma_S + \Gamma_R \cos(\theta + \varphi), \tag{31}$$

and allows us to treat the problem within the Hamiltonian formalism. Above, φ is just a phase. The amplitude of the resonant argument Eq. (3)

$$|A_R| = \frac{\Gamma_R}{a}\frac{1}{2}|T_k(e)| \tag{32}$$

with

$$T_k = \frac{1}{\pi}\int_0^{2\pi} \mathrm{d}\tilde{l}\left(\frac{a}{r}\right)\cos k\tilde{l}. \tag{33}$$

With the use of Eq. (7), one has for the semi-major axis width of the resonance

$$\Delta a_k = \epsilon\, a_R(k)\,\sqrt{|T_k|}, \quad \epsilon = \sqrt{\frac{8}{3}\frac{\Gamma_R}{\mu_c}}. \tag{34}$$

The k'th and the $k+1$'th resonance cross at an eccentricity $e_k = e_k(1/\epsilon)$ which satisfy

$$k^{2/3}\sqrt{|T_k(e_k)|} + (k+1)^{2/3}\sqrt{|T_{k+1}(e_k)|} = \frac{1}{\epsilon}[(k+1)^{2/3} - k^{2/3}]. \tag{35}$$

As before, we define a close approach parameter Π_k which corresponds to Ω_k of Eq. (16). This yields

$$\begin{aligned}\frac{\Pi_k}{\kappa\epsilon} &= \frac{1}{\kappa\epsilon}\frac{1-e_k}{1+e_k}\left[\kappa k^{2/3} + \epsilon a_R(k)\sqrt{|T_k(e_k)|}\right] \\ &= \frac{1-e_k}{1+e_k}k^{2/3}\left[\frac{1}{\epsilon} + \sqrt{|T_k(e_k)|}\right],\end{aligned} \tag{36}$$

and is plotted in Fig. 6 for $k = 5 \rightarrow 25$ in steps of 5. Here, the curves are defined to be zero whenever $e_k > 0.7$ which from studies is a conservative value for the divergence of the appropriate expansion of true anomaly in mean anomaly, with coefficients given by Eq. (33). From Fig. 6, one can see that if the pericenter distance is chosen to lie above

$$q > 2(1+e)\,\kappa_{j=1}, \quad e < 0.7, \tag{37}$$

the orbit should be "safe".

For instance, take an outgassing pressure field with a stationary and variable part which in strength are about one tenth of the gravitational attraction $\Gamma_S = \Gamma_R = 0.1\, r_c^3\, h^{-2}$ where h here represents an hour, which gives $\epsilon^{-1} = 2.0$. From Fig. 6, a safe Π should lie between $\Pi \sim (1.5$–$1.75)\,\kappa_{j=1}$, which we have compared with simulations, Fig. 7. The comparison is more ambiguous this time although there are some properties of the plot which are at terms with the presented theory.

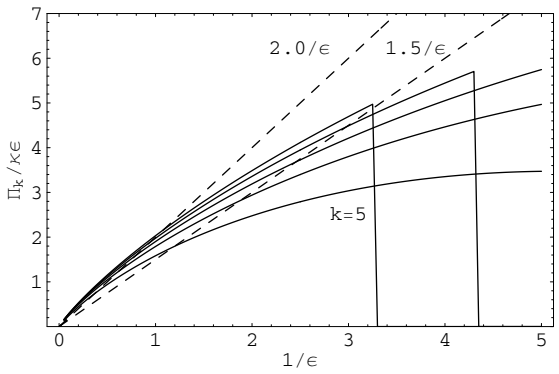

Fig. 6. Scaled approach parameter Π_k as function of the outgassing resonance strength parameter ϵ where $k = 5$, 10, 15, 20 and 25 is from bottom to top as usual. The range $1/\epsilon < 1$ is of very limited interest.

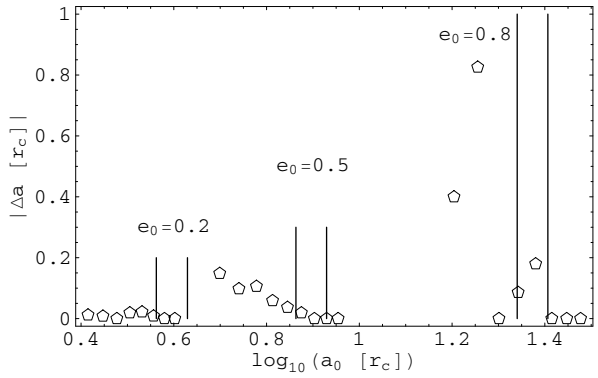

Fig. 7. Simulation series of the difference in semi-major axis induced by a pericenter passage of the probe are shown as a functions of the probe orbit's initial semi-major axis. The orbit elements are chosen to be $I_0 = g_0 = h_0 = 0$. The vertical bars, given in pairs for each series separated by different initial eccentricities, represent the boundaries within which we expect shape instability of the orbit to incur.

5. Radiation pressure resonances

Photons are absorbed by large solar cell arrays of Rosetta and constitute a significant perturbation of the spacecraft's orbit at all heliocentric distances. The corresponding acceleration is derivable from the potential

$$V_1 = -\frac{\xi}{R^2} r[\cos\lambda\cos u - \sin\lambda\sin u\cos I] \tag{38}$$

where ξ is a strength parameter dependent on the probe area which is exposed to solar radiation. The heliocentric distance of the comet is represented by R, r is the distance between the comet's mass center and probe while $u = f + g$ equals the sum of the orbiter's true anomaly f and argument of pericenter g. The angle $\lambda = h - \nu$ above is the difference, in the orbit plane of the comet, between the cometocentric orbit's longitude of ascending node h and the comet's heliocentric true anomaly ν (see for instance Mysen & Aksnes 2006). At last I here is the inclination of the spacecraft's orbit relative to the orbit plane of the comet.

Let Rosetta's large solar cell arrays rotate with respect to the Sun with a single frequency $\omega = \dot{\theta}$

$$\xi = \xi_S + \xi_R\cos(\theta + \varphi). \tag{39}$$

In the same way as before, we can deduce a Fourier amplitude

$$|A_R| = \frac{\xi_R}{R^2} a\,\Theta(I)\frac{1}{2}|S_k(e)|, \quad j = 1 \tag{40}$$

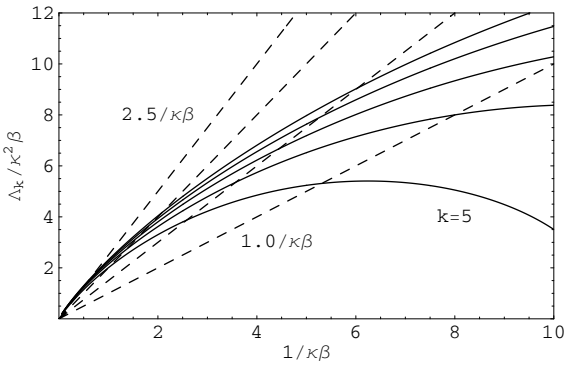

Fig. 8. The parameter Λ_k, which is expected to separate regular from chaotic motion, is plotted for different resonances and resonance strengths (through β) and rotation period of the solar cell arrays (through κ).

where the integer j again is the one of Eq. (5). The inclination dependent function is

$$\Theta = \sqrt{\cos^2\lambda + \sin^2\lambda\cos^2 I} \tag{41}$$

and for the part which is dependent on the orbit eccentricity

$$S_k = \frac{1}{\pi}\int_0^{2\pi} \mathrm{d}\tilde{l}\left(\frac{r}{a}\right)\cos f\cos k\tilde{l}. \tag{42}$$

The resonance widths go as

$$\Delta a_k = \beta\sqrt{|S_k|}\,a_R(k)^2, \quad \beta^2 = \frac{8}{3\mu_c}\frac{\xi_R}{R^2}\Theta, \tag{43}$$

and they cross at an eccentricity $e_k = e_k(1/\kappa\beta)$ from

$$k^{4/3}\sqrt{|S_k(e_k)|} + (k+1)^{4/3}\sqrt{|S_{k+1}(e_k)|} = \frac{1}{\kappa\beta}[(k+1)^{2/3} - k^{2/3}]. \tag{44}$$

Again, the universality of an overlap equation can be investigated

$$\frac{\Lambda_k}{\kappa^2\beta} = \frac{1-e_k}{1+e_k}\left[\frac{1}{\kappa\beta}k^{2/3} + k^{4/3}\sqrt{|S_k(e_k)|}\right], \tag{45}$$

and is plotted in Fig. 8 for the usual $k = 5 \rightarrow 25$ in steps of 5. The derivatives of the dashed lines included in the plot for reference increase in steps of 0.5. From the plot,

$$q > 2.5\,(1+e)\,\kappa_{j=1} \tag{46}$$

should form a conservative stability condition. The $k = 1$ and $k = 2$ resonances are seen to go from overlap at zero eccentricity to full separation over the short parameter range $1/\kappa\beta = 2.0 \rightarrow 3.5$. That is, for $1/\kappa\beta > 3.5$, a rotation frequency of the solar cell arrays which corresponds to the probe's orbit period should not lead to an unpredictable orbit shape instability.

We demonstrate these considerations with some examples. Let the initial orbit elements of Rosetta relative to a nominal comet target be $\lambda = I = 0.5$, $e = 0.1$ and $a = 20\,r_c$ when the comet passes the heliocentric distance $R = 4$ AU in its eccentric orbit towards the Sun. At this cometocentric distance the orbit period, and rotation period of the solar cell arrays if these are rotated in pace with the spacecraft's orbit, is about $P \equiv 500$ h, which yields the initial resonances in semi-major axis and eccentricity space of Fig. 9. In reference to the parameterization of

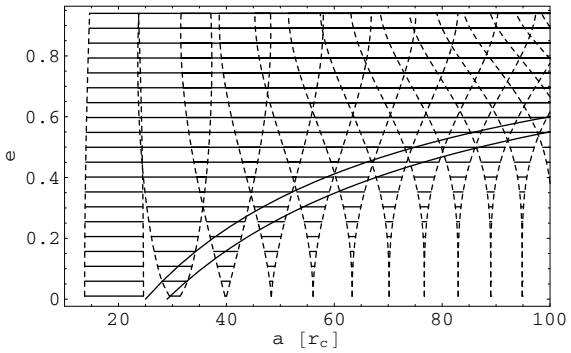

Fig. 9. Resonances in eccentricity and semi-major axis space for a probe started in an orbit away from the solar plane-of-sky at a comet heliocentric distance $R = 4$ AU. The solar cell arrays' rotation period is $P = 500$ h, and the curves defined by $\Lambda_5 = 25\,r_c$ and $\Lambda_{10} = 29\,r_c$, see Fig. 8, are included. In the presented semi-major axis range, the rotation period of the arrays is shorter than the initial cometocentric orbit period.

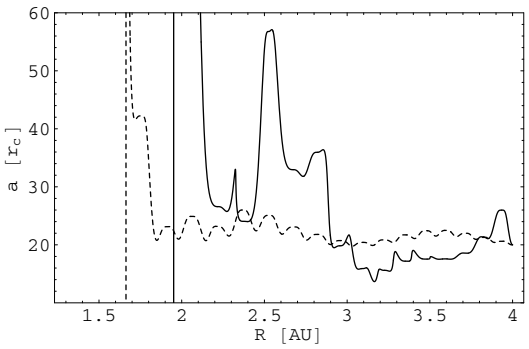

Fig. 10. Simulation results for two cometocentric trajectories around a nominal Rosetta target, and a spacecraft which initially rotates in pace with its motion in its orbit around the comet. Fairly consistent with Hamiltonian theory, aperiodic changes in the orbits shape occur when two resonances of the problem overlap. Escape is not solely dependent on this resonance problem alone.

Fig. 8, one then has the initial $1/\kappa\beta = 3.5$. As previously stated, the synchronous resonance, here at about $a = 20\,r_c$, is then separated from a neighbouring resonance, but this scenario deteriorates rapidly since $1/\kappa\beta \sim R$. It must also be pointed out that an initial low eccentricity does not help very much against aperiodic changes in the orbit's energy since it, for orbits started away from the so-called solar plane-of-sky with $I = \pi/2$ and $\lambda = \pm\pi/2$, executes large amplitude variations between a low value and $e \lesssim 1$, see for instance Mysen & Aksnes (2006). If one changes the initial inclination and relative node to for instance $I = -\lambda = 1.5$, one then has the initial $1/\kappa\beta = 11$, and the eccentricity will keep a low value under secular motion, which both are beneficial in order to avoid a resonance overlap instability.

Figure 10 shows the results of simulations of these two scenarios with a spacecraft mass to area factor of 20 kg m^{-2}, as it is defined for Fig. 9. The dashed curve represents the orbit which is started closest to the solar plane-of-sky, and it is the closest of the two to represent regular motion for which the semi-major axis is not to experience any secular change, a property connected to the periodic Hamiltonian nature of radiation pressure (Mysen & Aksnes 2006). However, even this orbit experiences a long periodic variation in semi-major axis in addition to that induced by the spacecraft in its orbit around the comet. Here, we interpret these in context of the synchronous resonance in which the probe is initially placed.

6. Conclusions

Within the simplified framework of the first fundamental model of resonance, the pendulum, we have studied several spin-orbit resonances which ESA's probe Rosetta could encounter in the vicinity of the target comet 67P/Churyumov-Gerasimenko. The intent was to find orbits which do not translate into two or more simultaneous librators, trajectories which therefore are not expected to yield rapid and, to some extent, unpredictable changes in the orbit's shape. In this paper we were not so concerned with the resonance interactions in regions were the pendulum model is of limited value, but focused on how the almost discrete stability limit between the two classes of trajectories changed with increasing orbit ellipticity.

First, the strongest spin-orbit resonances induced by a rotating comet nucleus shaped like a triaxial ellipsoid with constant mass density were considered. The study showed that a certain representation of the boundary between the shape stable and rapidly shape unstable trajectories could be expressed by a simple law in a parameter range relevant for the Rosetta mission. Accordingly, whenever the intrinsic parameters of the system are beneficial from the resonance overlap avoidance point-of-view, like for instance if nucleus mass and rotation period are small, it is more difficult to improve orbit stability with a proper choice of orbit.

An identical analysis of the strongest resonances generated by the mass irregularities of the nucleus yielded similar results. An important difference is that the relevant order of the gravity field could destroy shape stable orbits further out than what the resonances induced by the regular mass distribution did.

A class of resonant couplings between the spacecraft's cometocentric orbit and temporal variations of the outgassing pressure field connected to the nucleus' rotation, was also explored, as was the stability boundary created by the rotation of the probe's large solar cell arrays exposed by radiation from the Sun. Conservative stability bounds were derived in both cases.

Acknowledgements. This work was financed by the Research Council of Norway, project 170870.

References

Crifo, J. F., & Rodionov, A. V. 1997, Icarus, 129, 72
Crifo, J. F., Lukyanov, G. A., Zakharov, V. V., et al. 2004, in The New ROSETTA Targets, ed. L. Colangeli, E. M. Epifani, & P. Palumbo (Dordrecht: Kluwer), ASSL, 311, 119
Davidsson, B. J. R., & Gutiérrez, P. J. 2005, Icarus, 176, 453
Fulle, M., Barbieri, C., Cremonese, G., et al. 2004, A&A, 422, 357
Goldstein, H. 1980, Classical Mechanics (Reading: Addison-Wesley)
Heiskanen, W. A., & Moritz, H. 1967, Physical Geodesy (San Francisco: W.H. Freeman and Company)
Kinoshita, H., Hori, G., & Nakai, H. 1974, Modified Jacobi polynomials and its applications to expansions of disturbing functions. Annals of the Tokyo Astronomical Observatory, Second Series, Vol. XIV N.1
Kossacki, K. J., & Szutowicz, S. 2006, Planet. Space Sci., 54, 15
Lamy, P. L., Toth, I., Weaver, H., et al. 2003, The nucleus of comet 67P/Churyumov-Gerasimenko, the new target of the Rosetta mission, DPS 35th Meeting
Muinonen, K., & Lagerros, J. S. V. 1998, A&A, 333, 753
Mysen, E., & Aksnes, K. 2006, A&A, 455, 1143
Mysen, E., Olsen, Ø., & Aksnes, K. 2006, Planet. Space Sci., 54, 750
Olsen, Ø. 2005, A&A, 449, 821
Pätzold, M., Häusler, B., Aksnes, K., et al. 2006, Rosetta Radio Science Investigations (RSI), Space Sci. Rev., accepted
Rickman, H., Kamél, L., Festou, M. C., et al. 1987, ESA SP-278, 471
Stoer, J., & Bulirsch, R. 1980, in Introduction to Numerical Analysis (New York: Springer-Verlag), Chap. 7